Colloids and Surfaces A: Physicochemical and Engineering Aspects 631 (2021) 127687

Contents lists available at ScienceDirect

Colloids and Surfaces A: Physicochemical and Engineering Aspects

journal homepage: www.elsevier.com/locate/colsurfa

Highly efficient removal of Pb(II) and Cd(II) ions using magnesium hydroxide nanostructure prepared from seawater bittern by electrochemical method

Hanif Amrulloh [a,*], Yehezkiel Steven Kurniawan [b], Chairul Ichsan [c], Jelita Jelita [d], Wasinton Simanjuntak [e], Rudy Tahan Mangapul Situmeang [e], Philip Anggo Krisbiantoro [f,g]

[a] Department of Islamic Primary School Teacher Education, Institute for Islamic Studies Ma'arif NU (IAIMNU) Metro Lampung, Metro 34111, Indonesia
[b] Department of Chemistry, Universitas Gadjah Mada, Yogyakarta 55281, Indonesia
[c] Department of Chemistry, Raden Fatah Islamic State University, Palembang 30126, Indonesia
[d] IAIN Langsa, Langsa 24411, Indonesia
[e] Department of Chemistry, Universitas Lampung, Bandar Lampung 35141, Indonesia
[f] International Graduate Program of Molecular Science and Technology (NTU-MST), National Taiwan University, Taipei 10617, Taiwan
[g] Molecular Science and Technology, Taiwan International Graduate Program, Academia Sinica, Taipei 11529, Taiwan

GRAPHICAL ABSTRACT

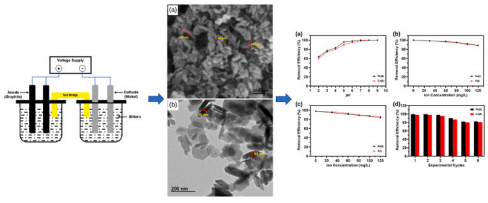

ARTICLE INFO

Keywords:
Magnesium hydroxide
Electrochemical synthesis
Pb(II)
Cd(II)
Adsorption
Wastewater treatment

ABSTRACT

In this work, we successfully synthesized magnesium hydroxide ($Mg(OH)_2$) nanostructure from seawater bittern by electrochemical method. The synthesis was performed at room temperature employing graphite and nickel as anode and cathode, respectively, without any pH adjustment. The $Mg(OH)_2$ nanomaterial was obtained in platelet form with length and thickness dimensions of 100–200 and 30–50 nm, respectively. From the surface analysis, the as-synthesized $Mg(OH)_2$ nanomaterial has a large surface area (193.7 $m^2\ g^{-1}$) and high pore volume (0.563 $cm^3\ g^{-1}$), thus promising to be used as the adsorbent for the removal of Pb(II) and Cd(II) ions. Kinetics analyses show that these heavy metal ions followed the pseudo-second-order model with a rate constant (k_{2p}) of 2.27×10^{-5} and 2.52×10^{-5} g mg^{-1} min^{-1} for Pb(II) and Cd(II) ions, respectively. Meanwhile, the maximum adsorption capacity (q_{max}) according to the Langmuir isotherm model for Pb(II) and Cd(II) ions was estimated to be 4.03×10^3 and 2.98×10^3 mg g^{-1}, respectively. These remarkable q_{max} values were mainly driven by a large surface area and high pore volume of the as-synthesized material. Furthermore, the material can be remarkably reused for at least six consecutive cycles without significant loss in the adsorption capacity. This work is capable of providing highly efficient removal of heavy metal ions route by utilizing a low cost and highly reusable nanostructured $Mg(OH)_2$, shows promising prospects for further large-scale applications.

* Corresponding author.
E-mail address: amrulloh.hanif@iaimnumetrolampung.ac.id (H. Amrulloh).

https://doi.org/10.1016/j.colsurfa.2021.127687
Received 30 August 2021; Received in revised form 2 October 2021; Accepted 5 October 2021
Available online 9 October 2021

1. Introduction

Water is critical for the existence of living beings [1–3]. Especially for mankind, water is substantially the root of public healthiness, and therefore access to clean water is indispensable to achieve public welfare. However, serious water pollution has recently become a persistent problem around the world owing to rapid population growth, urbanization, industrialization and massive agricultural activities [4–7]. In fact, ca. 40% of the lakes and the rivers around the world have been polluted with heavy metals [8]. Among heavy metals, lead (Pb(II)) and cadmium (Cd(II)) ions are widely found in aquatic samples in high concentrations [9]. It should be noted that even at a low concentration, these heavy metal ions can cause severe problems on human health, e.g., cancer, damages to the respiratory, anemia, neurological disorders, and multiorgan failure [10–13]. Therefore, World Health Organization (WHO) has limited the maximum concentration of Pb(II) and Cd(II) ions in drinking water to 0.010 and 0.005 mg L^{-1}, respectively [14]. Thence, the removal of Pb(II) and Cd(II) ions from wastewater is critical for the development of adequate water resources.

Several techniques have been widely reported for the treatment of wastewater containing Pb(II) and Cd(II) ions, including adsorption [15], chemical precipitation [16], coagulation [17], membrane filtration [18], ion-exchange [19], reverse osmosis [20], and electrochemistry [21]. These techniques, however, suffer from major drawbacks. For instance, a large amount of coagulant is added for chemical coprecipitation and coagulation techniques, while reverse osmosis is an expensive and slow output process. Meanwhile, electrochemistry technique requires high energy for the electrocoagulation process. Therefore, considerable attention has recently been given to adsorption owing to the simple operation of the technique, cost-effective, low energy demand and feasible for large-scale applications [15].

Many materials prepared have been reported for the adsorption of Pb (II) and Cd(II) ions, e.g., carbon [22], clays [23,24], layered double hydroxide [25], metal-organic framework [26], peat soil [27], and metal hydroxides and oxides [28]. Among them, metal hydroxides and metal oxides are much preferable for the removal of heavy metals due to their practicality for industrial-scale applications [29]. Several adsorbents based on metal hydroxide and metal oxide have been prepared from natural resources and/or urban mines, such as magnesium hydroxide ($Mg(OH)_2$) [30], magnesium oxide (MgO) [31], zinc oxide (ZnO) [32], magnetite (Fe_3O_4) [33], and titanium dioxide (TiO_2) [34]. These materials, however, possessed relatively low adsorption capacity and thence an adsorbent with higher adsorption capacity is keenly desired to achieve high adsorption efficiency.

$Mg(OH)_2$ nanostructure have recently been reported as a good adsorbent for the removal of both organic and inorganic pollutants [35,36]. This due to the fact that $Mg(OH)_2$ generally exhibits high specific surface area and thus it usually also possesses high adsorption capacity. Liu et al. reported that $Mg(OH)_2$ nanostructure exhibited 90% adsorption efficiency for Cr(IV) ions with good reusability (5 cycles) [37]. Guo et al. and Jiang et al. also reported that $Mg(OH)_2$ nanostructure able to remove 93% of Co(II) and Ni(II) ions from an aqueous solution within 50 min [38].

Generally, $Mg(OH)_2$ can be prepared by using several techniques, including electrochemical [39], precipitation [40], solvothermal [41], sonochemistry [42], and microwave-assisted process [43]. Among these preparation techniques, the electrochemical method is the one of the widely used due to the possibility for the usage of natural resources, such as seawater bittern. During the electrochemical process, the Mg(II) ions in the solution are converted into solid $Mg(OH)_2$ nanostructure [44,45]. Since to the best of our knowledge, the application of $Mg(OH)_2$ nanostructure prepared from natural seawater bittern source through an electrochemical method for the removal of Pb(II) and Cd(II) ions has not been reported yet, here we investigated the adsorption performance of the electrochemically synthesized $Mg(OH)_2$ nanostructure for the removal of the as-mentioned metal ions. In the present study, the effect of pH, reaction time and the concentration of Pb(II) and Cd(II) ions are the main focus of our work. While the reaction rate and the adsorption capacity were estimated, the adsorption mechanism was elucidated. Moreover, the effect of the coexisting metal ions and reusability of the as-prepared material were also highlighted.

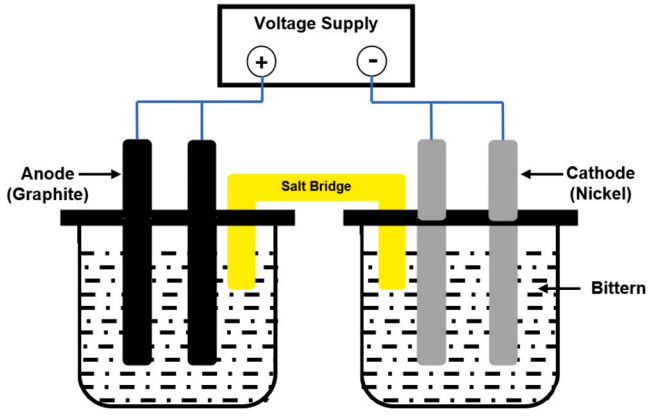

Fig. 1. Schematic process of the electrochemical synthesis of $Mg(OH)_2$ nanostructure.

2. Materials and methods

2.1. Materials

Bittern sample was obtained from salt farm in Pamekasan, Madura island, Indonesia. Other chemicals, e.g., gelatin powder, sodium chloride (NaCl), potassium chloride (KCl), sodium hydroxide (NaOH), hydrochloric acid (HCl), lead(II) nitrate ($Pb(NO_3)_2$), and cadmium(II) nitrate tetrahydrate ($Cd(NO_3)_2{\cdot}4H_2O$) were of analytical grade purchased from Sigma-Aldrich Reagent Pte. Ltd., Singapore. All chemicals were used without any further purification.

2.2. Preparation and characterization of $Mg(OH)_2$ nanostructure

The preparation of $Mg(OH)_2$ nanostructure was conducted in a similar manner to that the previously described in [45,46]. The electrochemical process employed a two-compartment electrochemical cell connected by a salt bridge (gelatin and NaCl suspension) with graphite and nickel as the cathode and anode, respectively. The schematic process of the electrochemical method is shown in Fig. 1. Bittern samples were diluted four times with deionized water without any pH adjustment and then the electrolysis process was performed at 18 V for 4h at room temperature. The resulting solid at the cathode was filtered and washed three times with deionized water. Afterward, the as-synthesized $Mg(OH)_2$ nanostructure was dried and characterized with a scanning electron microscope (SEM, FEI Inspect-S50) and transmission electron microscope (TEM, JEOL JEM-1400). SEM and TEM analyses were conducted to visualize the morphology and size of $Mg(OH)_2$ nanostructure. The surface area and porosity of the $Mg(OH)_2$ nanostructure was analyzed by nitrogen (N_2) gas isotherm adsorption at 77 K through surface analysis using BET technique (BET, Micromeritics TRIstar 3020). Meanwhile, the diffractogram of $Mg(OH)_2$ nanostructure was recorded with a continued scanning for 2° min^{-1} by using X-ray diffraction spectrometer (XRD, Expert Pro PANAnalytical) with Cu Kα radiation at 1.5406 Å (40 kV and 30 mA).

2.3. Batch adsorption experiment

The adsorption performance of $Mg(OH)_2$ nanostructure was evaluated through a batch adsorption process. The stock solutions of heavy metal ions were prepared by dissolving the nitrate metal salts with

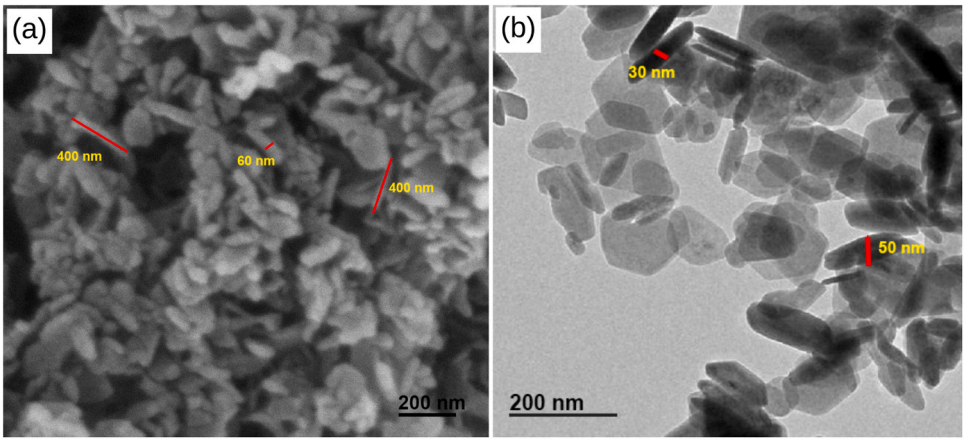

Fig. 2. (a) SEM and (b) TEM images of the as-synthesized $Mg(OH)_2$ nanostructure.

deionized water to obtain a concentration of 6×10^3 mg L^{-1}. The effect of initial pH, time, and initial concentration were performed to optimize the adsorption condition. All of the experiments were carried out in three replications at 298 K for 4 h employing 100 mg adsorbent. The pH value of the aqueous solution was adjusted by the addition of 0.1 -mol L^{-1} NaOH or 0.1 mol L^{-1} HCl. The concentration of metal ions was analyzed by using Inductively Coupled Plasma Optical Emission Spectroscopy (ICP-OES, Varian 715-ES). Meanwhile, the adsorption capacity (q_e, mg g^{-1}) and removal percentage (E, %) were calculated by using Eqs. (1) and (2) as follows:

$$q_e = \frac{(C_o - C_e)}{m} \times V \quad (1)$$

$$E = \frac{(C_o - C_e)}{C_o} \times 100\% \quad (2)$$

whereas, C_o and C_e are metal concentrations before and after the adsorption process (mg L^{-1}), respectively; V is the volume of aqueous solution (mL); and m is the mass of adsorbent [47].

3. Results and discussions

3.1. Characterizations of $Mg(OH)_2$ nanostructure

In this work, 30.45 g of $Mg(OH)_2$ nanostructure was produced from one liter of seawater bittern. The surface morphology of the as-synthesized $Mg(OH)_2$ was then observed by using SEM and TEM as shown in Fig. 2(a) and (b), respectively. As displayed in Fig. 2(a), the nanomaterial is composed of particles of different sizes and shapes. In general, the nanomaterial was obtained in elongated flat shapes with length of 100–400 nm and thickness of 20–65 nm. On the other hand, Fig. 2(b) shows that the nanomaterial was formed in plates with length of 100–200 nm and thickness of 30–50 nm. This result was in agreement with the previously reported $Mg(OH)_2$ nanomaterial with length of 100–200 nm and thickness of around 10 nm prepared by solid-state reaction [38].

The adsorption-desorption isotherm of N_2 gas for $Mg(OH)_2$ nanostructure is shown in Fig. S1(a). The as-produced $Mg(OH)_2$ nanostructure gave a characteristic of isotherm IV at medium to high pressure with an H3 hysteresis loop. The adsorption hysteresis loop was found at the center with unparalleled two branches indicating the porous structure of $Mg(OH)_2$ which is in agreement with the SEM micrograph (Fig. 2a). The pore distribution of nanostructured $Mg(OH)_2$ was found in a range of 5–45 nm (Fig. S1(b)) which was characteristic of mesopore structure. From the surface analysis, the surface area and pore volume of nanostructured $Mg(OH)_2$ were 193.7 m^2 g^{-1} and 0.563 cm^3 g^{-1}, respectively. Table 1 shows the comparison of the surface area of some reported adsorbents, whereas the surface area of the as-prepared $Mg(OH)_2$ in this work is higher than thermally and chemically treated clay, ZnO nanoflower, and nano $CaCO_3$ materials. Furthermore, it shall be noted that the as-prepared $Mg(OH)_2$ nanostructure in this work exhibited 1.2 times higher surface area and comparable pore volume compared to that of citric acid-functionalized $Mg(OH)_2$ (159.0 m^2 g^{-1}, 0.740 cm^3 g^{-1}) [48]. Moreover, the surface area of the prepared nanostructured $Mg(OH)_2$ in this work was also 2.7 times higher than the

Table 1
Comparison of the adsorption characteristics of Pb(II) and Cd(II) ions on the as-synthesized $Mg(OH)_2$ nanostructure.

Adsorbent	Surface area (m^2 g^{-1})	Pore Volume (cm^3 g^{-1})	q_{max} (mg g^{-1})		Ref.
			Pb (II)	Cd (II)	
Thermally and chemically treated clay	70.91	0.158	52.63	24.45	[50]
Mesoporous carbon stabilized alumina	415.2	0.530	235.6	49.98	[51]
Ni-P microstructure	425.0	–	39.00	40.70	[52]
Flowerlike MgO	72.00	–	1980	1500	[49]
ZnO nanoflower	11.25	0.036	115.0	71.50	[53]
Nano $CaCO_3$	43.60	0.148	1179	821.0	[54]
$Mg(OH)_2$ functionalized citric acid	159.0	0.740	4545	3571	[48]
Nanostructure Mg $(OH)_2$	193.7	0.563	4117	3043	This work

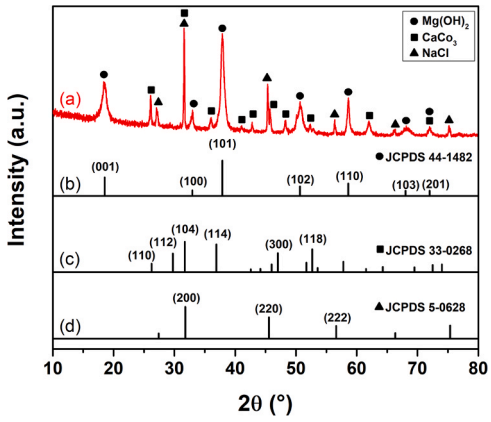

Fig. 3. XRD diffractogram of (a) $Mg(OH)_2$ nanostructure and the standard of (b) $Mg(OH)_2$, (c) $CaCO_3$ and (d) NaCl.

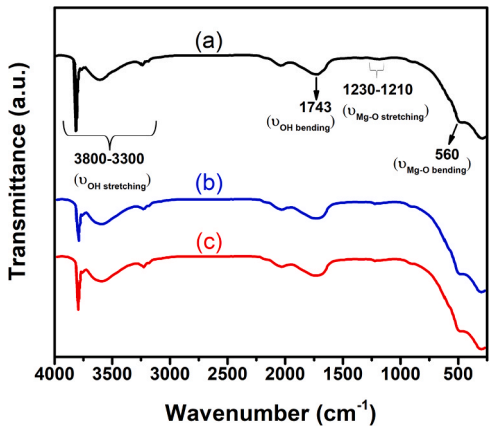

Fig. 4. FTIR spectra of $Mg(OH)_2$ nanostructure (a) before and after being used for the adsorption of (b) Pb(II) and (c) Cd(II) ions.

surface area of flowerlike MgO material (72 m^2 g^{-1}) [49].

To gain more detailed information on the crystal phase in the $Mg(OH)_2$ nanostructure, the XRD analysis was carried out in a 2θ range of 10–80°. The XRD analysis reveals the presence of $Mg(OH)_2$ (JCPDS, No. 44-1482) [48], $CaCO_3$ (JCPDS, No. 33-0268) [55], and NaCl (JCPDS, No. 5-0628) [56] crystal phases (see Fig. 3). The presence of $CaCO_3$ and NaCl crystal phases might due to the fact that the as-prepared $Mg(OH)_2$ nanostructure was electrochemically prepared from seawater bittern without any pre-treatment [57]. From the X-Ray Flouresence (XRF, PANAnalytical Epsilon 3) analysis, the $Mg(OH)_2$ nanostructure existed in 91% purity (Table S2).

The FTIR spectrum of nanostructured $Mg(OH)_2$ is shown in Fig. 4. The free and hydrogen-bonded O-H functional groups of $Mg(OH)_2$ were observed at 3700–3800 and 3300–3600 cm^{-1}, respectively [58]. The absorption signal of O–H bending and Mg–O stretching appeared at 1743 and 1210–1230 cm^{-1}, respectively. On the other hand, the Mg–O bending signal was found at below 600 cm^{-1} which was in agreement to the previous reported literature [59].

3.2. Adsorption of Pb(II) and Cd(II) ions by using $Mg(OH)_2$ nanostructure

3.2.1. Effect of pH

Initial pH is an important parameter in this study since it affects the surface charges of the as-synthesized adsorbent as well as the ionic speciation of Pb(II) and Cd(II) ions in the solution. To investigate the effect of pH on the adsorption percentages, $Mg(OH)_2$ nanostructure (100 mg) was added into the solution of Pb(II) or Cd(II) ion (100 mL, 1000 mg L^{-1}) at 298 K for 4 h. The pH of the solution was then adjusted to a predetermined value by the addition of 0.1 mol L^{-1} NaOH or HCl. It was observed that the removal percentages of either Pb(II) or Cd(II) ion increased by the increment of pH and then reached a plateau (Fig. 5(a)). Interestingly, approximately 60% removal of Pb(II) and Cd(II) ions was observed even at strong acidic condition (pH 2.0), demonstrating good adsorption performance of the as-synthesized $Mg(OH)_2$ nanostructure for the efficient removal of Pb(II) and Cd(II) ions. Complete removal of Pb(II) was achieved at pH 7.0, while complete removal of Cd(II) was achieved at pH 8.0. At these pH values, the hydroxyl groups of $Mg(OH)_2$ was deprotonated thus a complete Pb(II) and Cd(II) removal was achieved, which was in agreement with the previous report [48].

3.2.2. Effect of coexisting metal ions

It is well known that heavy metal ions may exist as a mixture with other coexisting metal ions, especially alkali metal ions [60]. Therefore, in this work, the effect of Na(I) and K(I) ions on the adsorption of Pb(II) and Cd(II) ions was evaluated and the results are shown in Fig. 5(b) and (c), respectively. It was revealed that the presence of either Na(I) or K(I) ion slightly decreased the adsorption percentages of Pb(II) (Fig. 5(b)) and Cd(II) (Fig. 5(c)) ions. As the adsorption of Pb(II) and Cd(II) ions occurred through an ion exchange reaction with the hydroxyl groups of $Mg(OH)_2$, it is reasonable that coexisting metal ions also slightly affect the adsorption percentages [49]. However, the adsorption percentages of Pb(II) and Cd(II) ions are still higher than 90% even at the highest concentration of coexisting metal ions, reflecting a good adsorption performance of $Mg(OH)_2$ for the removal of Pb(II) and Cd(II) ions from aqueous medium.

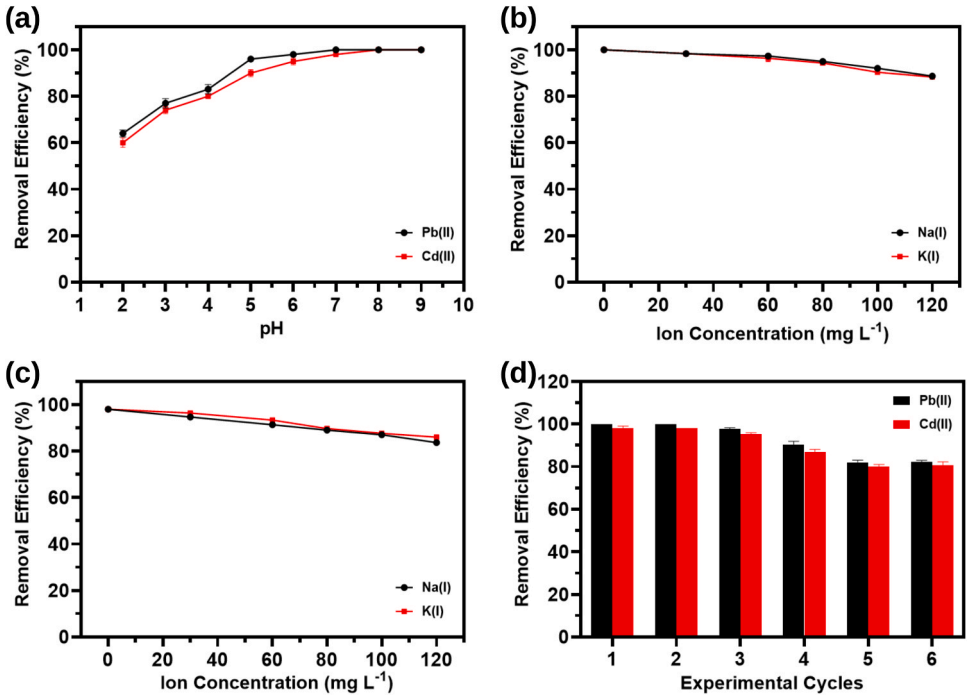

Fig. 5. (a) Effect of pH on the percent removal of Pb(II) and Cd(II) ions using $Mg(OH)_2$ nanostructure at 298 K; (b) Effect of coexisting metal ions on the removal efficiency of Pb(II) ion; (c) Effect of coexisting metal ions on the removal efficiency of Cd(II) ion; (d) Reusability test of the $Mg(OH)_2$ nanostructure.

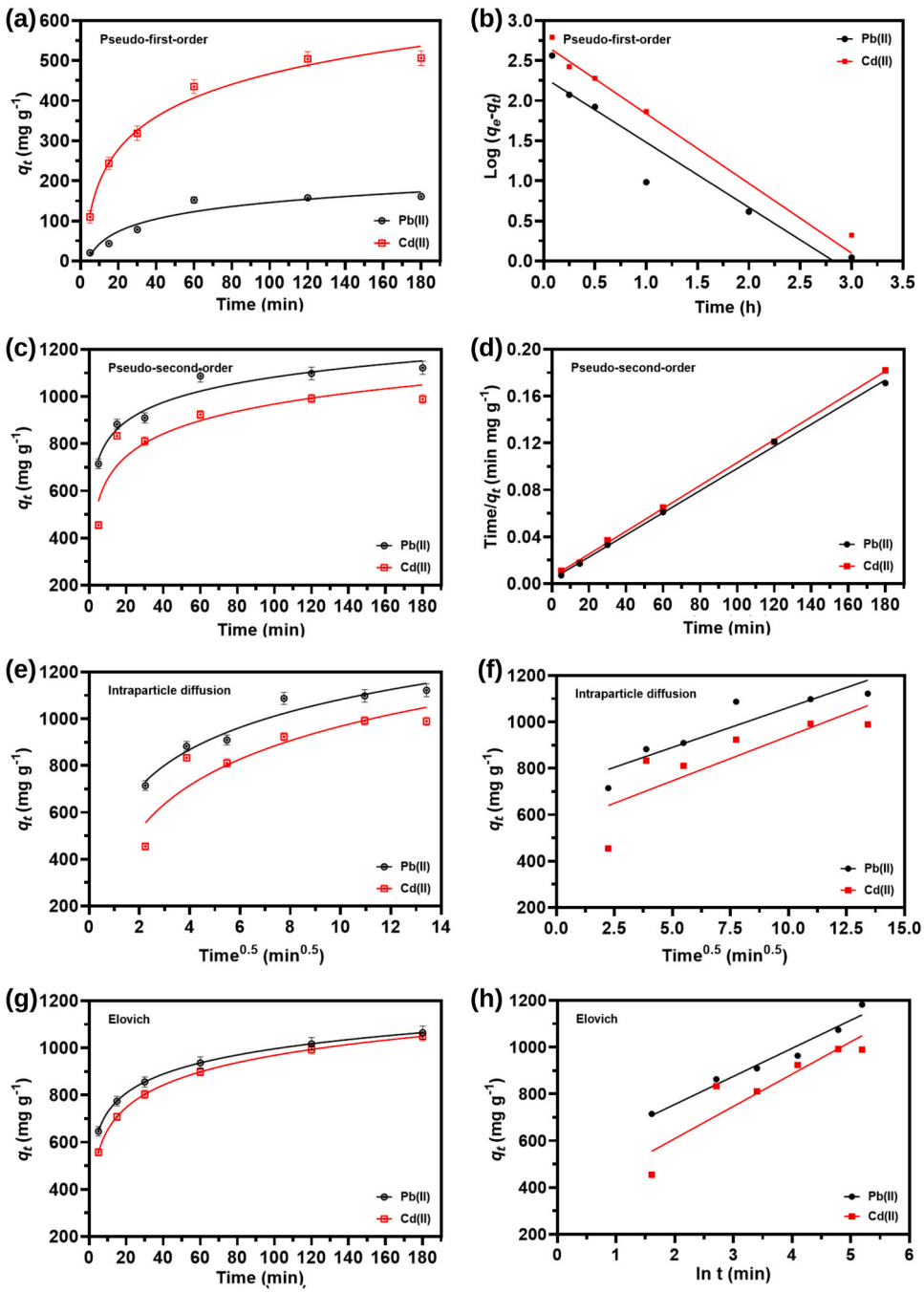

Fig. 6. Nonlinear and linear fitting of the removal of Pb(II) and Cd(II) ions on $Mg(OH)_2$ nanostructure using the (a, b) pseudo-first-order, (c, d) pseudo-second-order, (e, f) intraparticle diffusion and (g, h) Elovich kinetic models.

3.2.3. *Reusability and stability tests*

High adsorption performance and recyclability are critical parameters for an adsorbent so that is favorable for large-scale industrial processes [15]. Therefore, in this work, we investigated the reusability of the as-synthesized material (100 mg) for the removal of Pb(II) and Cd(II) ions with an initial concentration of 1.000×10^3 mg L^{-1} at pH 7.0. The regeneration of the adsorbent was conducted by simply washing the adsorbent with a diluted NaOH solution followed by deionized water. As shown in Fig. 5, the as-synthesized $Mg(OH)_2$ nanostructure can be reused for at least 6 times. During the first three cycles, no significant difference in the removal percentages of Pb(II) and Cd(II) ions was observed (Fig. 5(d)). At the fourth cycle, a slight decrement in the removal percentages of Pb(II) and Cd(II) was observed and then reached a plateau for the fifth and sixth cycles. The reason for the slight decrease in removal percentage of Pb(II) and Cd(II) ions after three cycles may be caused by the loss of a slight amount of adsorbent caused during the repeated adsorption process. However, it shall be noted that the $Mg(OH)_2$ nanostructure still exhibited high adsorption percentages and good reusability for Pb(II) and Cd(II) ions after six consecutive cycles, which is remarkable. Fig. 6 and 7.

3.3. *Adsorption kinetics*

The adsorption kinetics of Pb(II) and Cd(II) ions using $Mg(OH)_2$ nanostructure was evaluated by using pseudo-first-order, pseudo-second-order, intraparticle diffusion, and Elovich kinetic models [61]. As

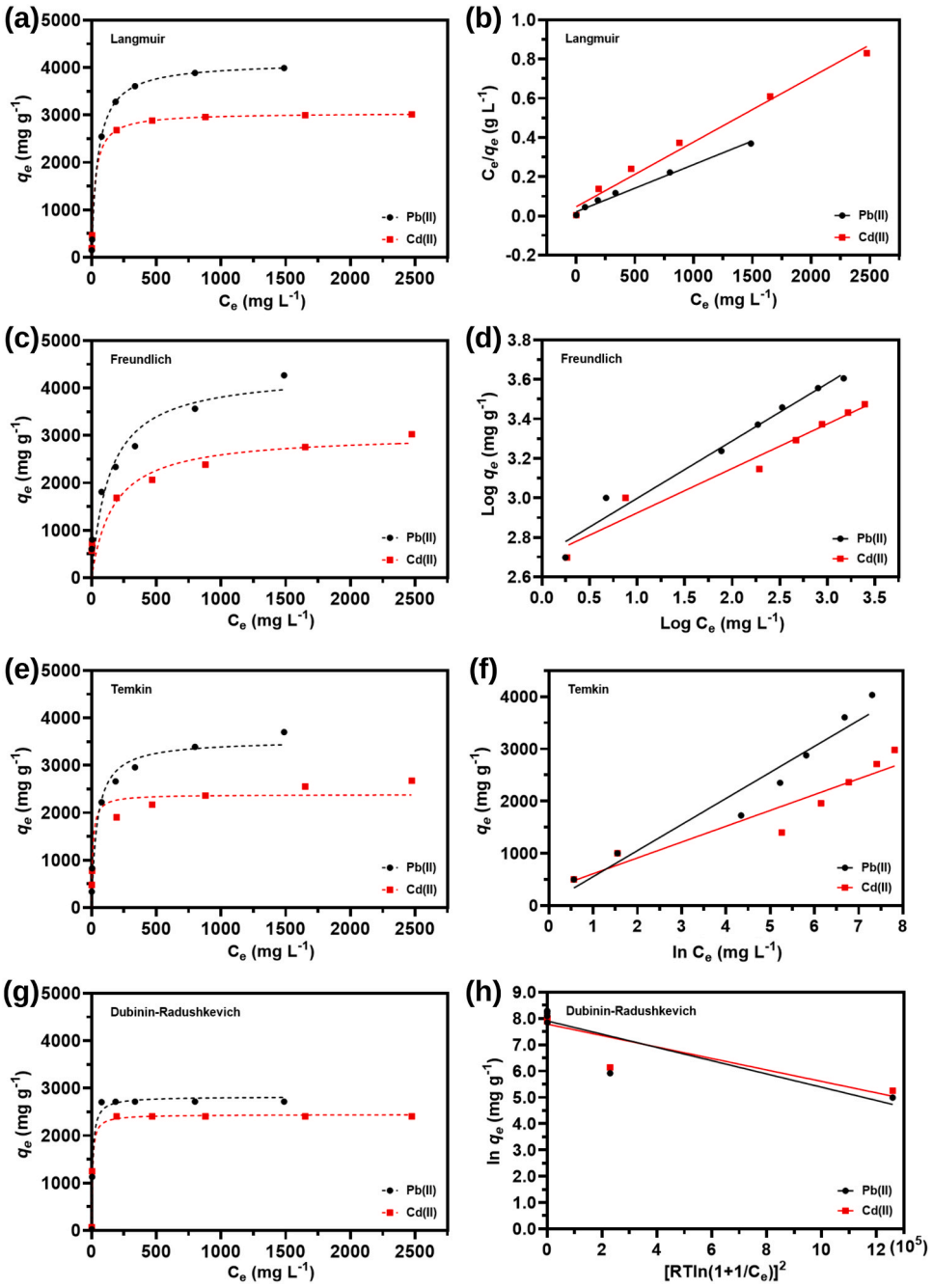

Fig. 7. Nonlinear and linear fitting of (a, b) Langmuir, (c, d) Freundlich, (e, f) Temkin, and (g, h) Dubinin-Radushkevich isotherm models for removal of Pb(II) and Cd(II) ions by using $Mg(OH)_2$ nanostructure.

shown in Table 2, both Pb(II) and Cd(II) ions adsorption kinetics followed the pseudo-second-order model with an R^2 value of 0.998 and 0.999, respectively, which was higher than pseudo-first-order, intraparticle diffusion, and Elovich models. This means that the adsorption of both Pb(II) and Cd(II) ions is governed by at least two parameters, plausibly the active sites of the adsorbent, i.e., –OH, and the concentration of the Pb(II) or Cd(II) ion. The interaction between the two may be then interpreted as a chemisorption process. This will further be discussed in the adsorption isotherms section. The adsorption rate constant of Pb(II) ion adsorption ($k_{2p} = 2.270 \times 10^{-5}$ g mg^{-1} min^{-1}) was slightly slower than that for Cd(II) ion adsorption ($k_{2p} = 2.520 \times 10^{-5}$ g mg^{-1} min^{-1}). Meanwhile, the theoretical q_e value for Pb(II) ion (1.087×10^3 mg g^{-1}) was higher than that for Cd(II) ion (0.833×10^3 mg g^{-1}). Furthermore, the theoretical q_e values for Pb(II) and Cd(II) ions were closed to the experimental q_e values of Pb(II) (9.997×10^2 mg g^{-1}) and Cd(II) (9.995×10^2 mg g^{-1}) ions, demonstrating the validity of the pseudo-second-order model.

3.4. Adsorption isotherms

The isotherm adsorption of Pb(II) and Cd(II) ions employing $Mg(OH)_2$ nanostructure as the adsorbent was evaluated by varying the initial concentration of metal ions ($0.500–6.000 \times 10^3$ mg L^{-1}) at a constant temperature (298 K). The experimental data were then plotted by using Langmuir, Freundlich, Temkin, and Dubinin-Raduskevich isotherm models [47]. The obtained isotherm parameters of Pb(II) and Cd(II) ions adsorption are listed in Table 3. The adsorption of both Pb(II) and Cd(II) ions fit well with the Langmuir model as shown by the R^2

Table 2
Kinetic parameters for the removal of Pb(II) and Cd(II) ions from aqueous solution by using $Mg(OH)_2$ nanostructure.

Kinetic models	Parameters	Heavy metal ions	
		Pb(II)	Cd(II)
Pseudo-first-order	k_{1p} (min^{-1})	1.880	2.010
	q_{th} (mg g^{-1})	161.8	508.3
	R^2	0.914	0.961
Pseudo-second-order	k_{2p} (g mg^{-1} min^{-1})	2.270×10^{-5}	2.520×10^{-5}
	q_e (mg g^{-1})	1.087×10^{2}	0.833×10^{2}
	R^2	0.998	0.999
Intraparticle diffusion	k_{IPD} (mg g^{-1} $min^{-0.5}$)	34.37	38.51
	C (mg g^{-1})	718.2	553.3
	R^2	0.835	0.675
Elovich	α (mg g^{-1} min^{-1})	6.394×10^{3}	1.540×10^{3}
	β (g mg^{-1})	7.881×10^{-3}	7.251×10^{-3}
	R^2	0.941	0.848

Table 3
Isotherm parameters for the removal of Pb(II) and Cd(II) ions from aqueous solution by using $Mg(OH)_2$ nanostructure.

Isotherm models	Parameters	Heavy metal ions	
		Pb(II)	Cd(II)
Langmuir	q_{max} (mg g^{-1})	4117	3043
	K_L	0.021	0.038
	q_e (mg g^{-1})	4033	2980
	R^2	0.987	0.984
Freundlich	log K_F (mg g^{-1} (mg $L^{-1})^{1/n}$)	2.710	2.700
	$1/n$	0.290	0.230
	R^2	0.973	0.958
Temkin	K_T (L mg^{-1})	1.110	2.750
	b (J mol^{-1})	4.990	8.230
	R^2	0.945	0.908
Dubinin-Radushkevich	K_{DR}	3.821×10^{-6}	2.863×10^{-6}
	q_m (mg g^{-1})	2715	2405
	R^2	0.774	0.802

value of 0.987 and 0.984, respectively, which was higher than Freundlich, Temkin, and Dubinin-Raduskevich models. It means that the adsorption of these heavy metal ions occurred through a chemisorption process on the surface of the adsorbent. The theoretical q_{max} value for Pb (II) (4,117 mg L^{-1}) and Cd(II) (3,043 mg L^{-1}) derived from the Langmuir model are close to the experimental q_{max} values of Pb(II) (4,033 mg L^{-1}) and Cd(II) (2,980 mg L^{-1}), respectively. Compared to the other adsorbent materials, the q_{max} value for Pb(II) and Cd(II) removal by using nanostructured $Mg(OH)_2$ was higher than mesoporous carbon stabilized alumina, flowerlike MgO, Ni-P microstructure, ZnO nanoflower, nano $CaCO_3$, and ZrMOFs functionalized NH_2, which is remarkable (Table 1). This higher adsorption capacity is most likely due to a large surface area and pore volume (Table 1). Even though the q_{max} value for Pb(II) and Cd (II) removal by using nanostructured $Mg(OH)_2$ is slightly lower than those reported for $Mg(OH)_2$ functionalized citric acid, the preparation of $Mg(OH)_2$ nanostructure in this work was simpler and lower-cost from seawater bittern sources. These findings demonstrate that the as-prepared $Mg(OH)_2$ nanostructure is a potential adsorbent material for an efficient Pb(II) and Cd(II) removal from the aqueous media.

3.5. Plausible adsorption mechanism

Fig. 4 shows the FTIR spectrum of $Mg(OH)_2$ nanostructure before and after the adsorption of Pb(II) and Cd(II) ions. The intensity of the O-H functional group of $Mg(OH)_2$ at 3800–3300 and 1743 cm^{-1} decreased after Pb(II) and Cd(II) adsorption indicating that the adsorption mechanism mainly occurred through ion-exchange reaction. Similar result was reported by Ponomarev et al. [62] for Ni(II), Cd(II), and Pb(II) adsorption using lignin-$Mg(OH)_2$ nanocomposite material. The plausible adsorption mechanism is shown in Fig. 8.

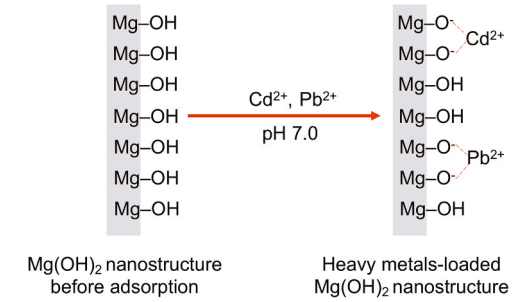

Fig. 8. Plausible adsorption mechanism of Pb(II) and Cd(II) ions on the $Mg(OH)_2$ nanostructure.

4. Conclusions

In summary, $Mg(OH)_2$ nanostructure is a promising adsorbent for the removal of Pb(II) and Cd(II) ions due to its high adsorption capacity and reusability. The $Mg(OH)_2$ nanostructure was successfully prepared through an electrochemical process from the natural seawater bittern. Characterizations of the material revealed the existence of $Mg(OH)_2$ in a nanostructured form with a large surface area and pore volume, resulting in remarkably high q_{max} value of 4.03×10^3 dan 2.98×10^3 mg g^{-1} for Pb(II) and Cd(II) ions, respectively. The adsorption kinetics followed the pseudo-second-order model with a rate constant (k_{2p}) of 2.27×10^{-5} and 2.52×10^{-5} g mg^{-1} min^{-1} for Pb(II) and Cd(II), respectively. These findings demonstrate that the as-prepared $Mg(OH)_2$ nanostructure from natural seawater bittern source shows promising prospects for further large-scale applications.

CRediT authorship contribution statement

H. Amrulloh: Investigation, Methodology, Data curation, Visualization, Writing – original draft. **Y.S. Kurniawan**: Data curation, Writing – review & editing. **C. Ichsan**: Writing – review & editing. **J. Jelita**: Writing – review & editing. **W. Simanjuntak**: Supervision, Conceptualization, Methodology. **R.T.M. Situmeang**: Supervision, Conceptualization. **P.A. Krisbiantoro**: Investigation, Visualization, Writing – review & editing.

Declaration of Competing Interest

The authors declare that they have no known competing financial interests or personal relationships that could have appeared to influence the work reported in this paper.

Acknowledgement

This work was financially supported by the Lembaga Penelitian dan Pengabdian Masyarakat (LP2M) Institute for Islamic Studies Ma'arif NU (IAIMNU) Metro Lampung, Indonesia (No: 07/0125/IAIMNU/LPM/XI/2020). Furthermore, acknowledgement is also expressed for the material characterization at the Integrated Laboratory and Center for Technology Innovation (LTSIT) The University of Lampung, Central Laboratory of Mineral and Advanced Material of Universitas Negeri Malang, and Department of Chemistry of Universitas Gadjah Mada.

Appendix A. Supporting information

Supplementary data associated with this article can be found in the online version at doi:10.1016/j.colsurfa.2021.127687.

References

[1] A. Gallego-Schmid, R.R.Z. Tarpani, Life cycle assessment of wastewater treatment in developing countries: a review, Water Res. 153 (2019) 63–69, https://doi.org/10.1016/j.watres.2019.01.010.

[2] Y. Jia, F. Zheng, H.R. Maier, A. Ostfeld, E. Creaco, D. Savic, J. Langeveld, Z. Kapelan, Water quality modeling in sewer networks: review and future research directions, Water Res. 202 (2021), 117419, https://doi.org/10.1016/j.watres.2021.117419.

[3] Y.S. Kurniawan, K.T.A. Priyangga, P.A. Krisbiantoro, A.C. Imawan, Green chemistry influences in organic synthesis: a review, J. Multidiscip. Appl. Nat. Sci. 1 (2021) 1–12, https://doi.org/10.47352/jmans.v1i1.2.

[4] L. Corominas, D.M. Byrne, J.S. Guest, A. Hospido, P. Roux, A. Shaw, M.D. Short, The application of life cycle assessment (LCA) to wastewater treatment: a best practice guide and critical review, Water Res. 184 (2020), 116058, https://doi.org/10.1016/j.watres.2020.116058.

[5] M.G. Uddin, S. Nash, A.I. Olbert, A review of water quality index models and their use for assessing surface water quality, Ecol. Indic. 122 (2021), 107218, https://doi.org/10.1016/j.ecolind.2020.107218.

[6] A. Fadaka, O. Aluko, S. Awawu, K. Theledi, Green synthesis of gold nanoparticles using *Pimenta dioica* leaves aqueous extract and their application as photocatalyst, antioxidant, and antibacterial agents, J. Multidiscip. Appl. Nat. Sci. 1 (2021) 78–88, https://doi.org/10.47352/jmans.v1i2.81.

[7] N. Zolkefli, S.S. Sharuddin, M.Z.M. Yusoff, M.A. Hassan, T. Maeda, N. Ramli, A review of current and emerging approaches for water pollution monitoring, Water 12 (2020) 3417, https://doi.org/10.3390/w12123417.

[8] C. Zamora-Ledezma, D. Negrete-Bolagay, F. Figueroa, E. Zamora-Ledezma, M. Ni, F. Alexis, V.H. Guerrero, Heavy metal water pollution: a fresh look about hazards, novel and conventional remediation methods, Environ. Technol. Innov. 22 (2021), 101504, https://doi.org/10.1016/j.eti.2021.101504.

[9] G.K. Kinuthia, V. Ngure, D. Beti, R. Lugalia, A. Wangila, L. Kamau, Levels of heavy metals in wastewater and soil samples from open drainage channels in Nairobi, Kenya: community health implication, Sci. Rep. 10 (2020) 8434, https://doi.org/10.1038/s41598-020-65359-5.

[10] S. Sobhanardakani, L. Tayebi, S.V. Hosseini, Health risk assessment of arsenic and heavy metals (Cd, Cu, Co, Pb, and Sn) through consumption of caviar of Acipenser persicus from Southern Caspian Sea, Environ. Sci. Pollut. Res. 25 (2018) 2664–2671, https://doi.org/10.1007/s11356-017-0705-8.

[11] W. Dong, Y. Zhang, X. Quan, Health risk assessment of heavy metals and pesticides: a case study in the main drinking water source in Dalian, China, Chemosphere 242 (2020), 125113, https://doi.org/10.1016/j.chemosphere.2019.125113.

[12] D. Aithani, D.S. Jyethi, Z. Siddiqui, A.K. Yadav, P.S. Khillare, Source apportionment, pollution assessment, and ecological and human health risk assessment due to trace metals contaminated groundwater along urban river floodplain, Groundw. Sustain. Dev. 11 (2020), 100445, https://doi.org/10.1016/j.gsd.2020.100445.

[13] R. Han, B. Zhou, Y. Huang, X. Lu, S. Li, N. Li, Bibliometric overview of research trends on heavy metal health risks and impacts in 1989–2018, J. Clean. Prod. 276 (2020), 123249, https://doi.org/10.1016/j.jclepro.2020.123249.

[14] WHO. Guidelines for Drinking Water Quality, fourth ed., WHO Press, Geneva, Switzerland, 2011.

[15] R. Yousef, H. Qiblawey, M.H. El-Naas, Adsorption as a process for produced water treatment: a review, Processes 8 (2020) 1657, https://doi.org/10.3390/pr8121657.

[16] Q. Chen, Y. Yao, X. Li, J. Lu, J. Zhou, Z. Huang, Comparison of heavy metal removals from aqueous solutions by chemical precipitation and characteristics of precipitates, J. Water Process Eng. 26 (2018) 289–300, https://doi.org/10.1016/j.jwpe.2018.11.003.

[17] Q. Zhang, X. Ye, H. Li, D. Chen, W. Xiao, S. Zhao, R. Xiong, J. Li, Cumulative effects of pyrolysis temperature and process on properties, chemical speciation, and environmental risks of heavy metals in magnetic biochar derived from coagulation-flocculation sludge of swine wastewater, J. Environ. Chem. Eng. 8 (2020), 104472, https://doi.org/10.1016/j.jece.2020.104472.

[18] J.E. Efome, D. Rana, T. Matsuura, C.Q. Lan, Experiment and modeling for flux and permeate concentration of heavy metal ion in adsorptive membrane filtration using a metal-organic framework incorporated nanofibrous membrane, Chem. Eng. J. 352 (2018) 737–744, https://doi.org/10.1016/j.cej.2018.07.077.

[19] M. Maslova, V. Ivanenko, N. Yanicheva, L. Gerasimova, The effect of heavy metal ions hydration on their sorption by a mesoporous titanium phosphate ion-exchanger, J. Water Process Eng. 35 (2020), 101233, https://doi.org/10.1016/j.jwpe.2020.101233.

[20] C. Vaneeckhaute, O. Darveau, E. Meers, Fate of micronutrients and heavy metals in digestate processing using vibrating reversed osmosis as resource recovery technology, Sep. Purif. Technol. 223 (2019) 81–87, https://doi.org/10.1016/j.seppur.2019.04.055.

[21] A. Yaqub, H. Ajab, S. Khan, S. Khan, R. Farooq, Electrochemical removal of copper and lead from industrial wastewater: mass transport enhancement, Water Qual. Res. J. 44 (2009) 183–188, https://doi.org/10.2166/wqrj.2009.020.

[22] Z. Zhang, T. Wang, H. Zhang, Y. Liu, B. Xing, Adsorption of Pb(II) and Cd(II) by magnetic activated carbon and its mechanism, Sci. Total Environ. 757 (2021), 143910, https://doi.org/10.1016/j.scitotenv.2020.143910.

[23] M.-Q. Jiang, X.-Y. Jin, X.-Q. Lu, Z.-L. Chen, Adsorption of Pb(II), Cd(II), Ni(II) and Cu(II) onto natural kaolinite clay, Desalination 252 (2010) 33–39, https://doi.org/10.1016/j.desal.2009.11.005.

[24] A. Sari, M. Tuzen, M. Soylak, Adsorption of Pb(II) and Cr(III) from aqueous solution on Celtek clay, J. Hazard. Mater. 144 (2007) 41–46, https://doi.org/10.1016/j.jhazmat.2006.09.080.

[25] D. Zhao, G. Sheng, J. Hu, C. Chen, X. Wang, The adsorption of Pb(II) on Mg_2Al layered double hydroxide, Chem. Eng. J. 171 (2011) 167–174, https://doi.org/10.1016/j.cej.2011.03.082.

[26] B.-L. Zhang, W. Qiu, P.-P. Wang, Y.-L. Liu, J. Zou, L. Wang, J. Ma, Mechanism study about the adsorption of Pb(II) and Cd(II) with iron-trimesic metal-organic frameworks, Chem. Eng. J. 385 (2020), 123507, https://doi.org/10.1016/j.cej.2019.123507.

[27] F. Qin, B. Wen, X.-Q. Shan, Y.-N. Xie, T. Liu, S.-Z. Zhang, S.U. Khan, Mechanisms of competitive adsorption of Pb, Cu, and Cd on peat, Environ. Pollut. 144 (2006) 669–680, https://doi.org/10.1016/j.envpol.2005.12.036.

[28] M. Kuang, Y. Shang, G. Yang, B. Liu, B. Yang, Facile synthesis of hollow mesoporous MgO spheres via spray-drying with improved adsorption capacity for Pb(II) and Cd(II), Environ. Sci. Pollut. Res. 26 (2019) 18825–18833, https://doi.org/10.1007/s11356-019-05277-2.

[29] L. Wang, C. Shi, L. Wang, L. Pan, X. Zhang, J.-J. Zou, Rational design, synthesis, adsorption principles and applications of metal oxide adsorbents: a review, Nanoscale 12 (2020) 4790–4815, https://doi.org/10.1039/C9NR09274A.

[30] V. Sirota, V. Selemenev, M. Kovaleva, I. Pavlenko, K. Mamunin, V. Dokalov, M. Yapryntsev, Preparation of crystalline $Mg(OH)_2$ nanopowder from serpentinite mineral, Int. J. Min. Sci. Technol. 28 (2018) 499–503, https://doi.org/10.1016/j.ijmst.2017.12.018.

[31] H. Amrulloh, A. Fatiqin, W. Simanjuntak, H. Afriyani, A. Annissa, Antioxidant and antibacterial activities of magnesium oxide nanoparticles prepared using aqueous extract of *Moringa oleifera* bark as green agents, J. Multidiscip. Appl. Nat. Sci. 1 (2021) 44–53, https://doi.org/10.47352/jmans.v1i1.9.

[32] V. Dhiman, N. Kondal, ZnO Nanoadsorbents: a potent material for removal of heavy metal ions from wastewater, Colloid Interface Sci. Commun. 41 (2021), 100380, https://doi.org/10.1016/j.colcom.2021.100380.

[33] S. Sobhanardakani, R. Zandipak, 2,4-Dinitrophenylhydrazine functionalized sodium dodecyl sulfate-coated magnetite nanoparticles for effective removal of Cd (II) and Ni(II) ions from water samples, Environ. Monit. Assess. 187 (2015) 412, https://doi.org/10.1007/s10661-015-4635-y.

[34] S. Sobhanardakani, R. Zandipak, Synthesis and application of $TiO_2/SiO_2/Fe_3O_4$ nanoparticles as novel adsorbent for removal of Cd(II), Hg(II) and Ni(II) ions from water samples, Clean. Technol. Environ. Policy 19 (2017) 1913–1925, https://doi.org/10.1007/s10098-017-1374-5.

[35] A. Jarosinski, P. Radomski, L. Lelek, J. Kulczycka, New production route of magnesium hydroxide and related environmental impact, Sustainability 12 (2020) 8822, https://doi.org/10.3390/su12218822.

[36] G. Balducci, L.B. Diaz, D.H. Gregory, Recent progress in the synthesis of nanostructured magnesium hydroxide, Cryst. Eng. Comm. 19 (2017) 6067–6084, https://doi.org/C7CE01570D.

[37] X. Liu, C. Liao, L. Lin, H. Gao, J. Zhou, Z. Feng, Z. Lin, Research progress in the environmental application of magnesium hydroxide nanomaterials, Surf. Interfaces 21 (2020), 100701, https://doi.org/10.1016/j.surfin.2020.100701.

[38] X. Guo, J. Lu, L. Zhang, Magnesium hydroxide with higher adsorption capacity for effective removal of Co(II) from aqueous solutions, J. Taiwan Inst. Chem. Eng. 44 (2013) 630–636, https://doi.org/10.1016/j.jtice.2012.12.020.

[39] G. Zou, R. Liu, W. Chen, Highly textural lamellar mesostructured magnesium hydroxide via a cathodic electrodeposition process, Mater. Lett. 61 (2007) 1990–1993, https://doi.org/10.1016/j.matlet.2006.07.172.

[40] D. Chen, L. Zhu, H. Zhang, K. Xu, M. Chen, Magnesium hydroxide nanoparticles with controlled morphologies via wet coprecipitation, Mater. Chem. Phys. 109 (2008) 224–229, https://doi.org/10.1016/j.matchemphys.2007.11.014.

[41] Y. Ding, G. Zhang, H. Wu, B. Hai, L. Wang, Y. Qian, Nanoscale magnesium hydroxide and magnesium oxide powders: control over size, shape, and structure via hydrothermal synthesis, Chem. Mater. 13 (2001) 435–440, https://doi.org/10.1021/cm000607e.

[42] M.A. Alavi, A. Morsali, Syntheses and characterization of $Mg(OH)_2$ and MgO nanostructures by ultrasonic method, Ultrason. Sonochem. 17 (2010) 441–446, https://doi.org/10.1016/j.ultsonch.2009.08.013.

[43] F. Al-Hazmi, A. Umar, G.N. Dar, A.A. Al-Ghamdi, S.A. Al-Sayari, A. Al-Hajry, S. H. Kim, R.M. Al-Tuwirqi, F. Alnowaiserb, F. El-Tantawy, Microwave assisted rapid growth of $Mg(OH)_2$ nanosheet networks for ethanol chemical sensor application, J. Alloy. Compd. 519 (2012) 4–8, https://doi.org/10.1016/j.jallcom.2011.09.089.

[44] H. Amrulloh, W. Simanjuntak, R.T.M. Situmeang, S.L. Sagala, R. Bramawanto, R. Nahrowi, Effect of dilution and electrolysis time on recovery of Mg^{2+} as $Mg(OH)_2$ from bittern by electrochemical method, J. Pure Appl. Chem. Res. 8 (2019) 87–95, https://doi.org/10.21776/ub.jpacr.2019.008.001.455.

[45] H. Amrulloh, W. Simanjuntak, R.T.M. Situmeang, S.L. Sagala, R. Bramawanto, A. Fatiqin, R. Nahrowi, M. Zuniati, Preparation of nano-magnesium oxide from Indonesia local seawater bittern using the electrochemical method, Inorg. Nano-Met. Chem. 50 (2020) 693–698, https://doi.org/10.1080/24701556.2020.1724146.

[46] W. Liu, F. Huang, Y. Wang, T. Zou, J. Zheng, Z. Lin, Recycling $Mg(OH)_2$ nanoadsorbent during treating the low concentration of Cr^{VI}, Environ. Sci. Technol. 45 (2011) 1955–1961, https://doi.org/10.1021/es1035199.

[47] C.P. Sagita, L. Nulandaya, Y.S. Kurniawan, Efficient and low-cost removal of methylene blue using activated natural kaolinite material, J. Multidiscip. Appl. Nat. Sci. 1 (2021) 69–77, https://doi.org/10.47352/jmans.v1i2.80.

[48] H. Zhu, L. Li, W. Chen, Y. Tong, X. Wang, Controllable synthesis of coral-like hierarchical porous magnesium hydroxide with various surface area and pore

volume for lead and cadmium ion adsorption, J. Hazard. Mater. 416 (2021), 125922, https://doi.org/10.1016/j.jhazmat.2021.125922.
[49] C.-Y. Cao, J. Qu, F. Wei, H. Liu, W.-G. Song, Superb adsorption capacity and mechanism of flowerlike magnesium oxide nanostructures for lead and cadmium ions, ACS Appl. Mater. Interfaces 4 (2012) 4283–4287, https://doi.org/10.1021/am300972z.
[50] S.I. Abu-Eishah, Removal of Zn, Cd, and Pb Ions from water by Sarooj clay, Appl. Clay Sci. 42 (2008) 201–205, https://doi.org/10.1016/j.clay.2008.02.003.
[51] Y.-F. Yang, X.-F. Wu, G.-S. Hu, B.-B. Wang, Effects of stearic acid on synthesis of magnesium hydroxide via direct precipitation, J. Cryst. Growth 310 (2008) 3557–3560, https://doi.org/10.1016/j.jcrysgro.2008.05.006.
[52] Y. Ni, K. Mi, C. Cheng, J. Xia, X. Ma, J. Hong, Urchin-like Ni–P microstructures: facile synthesis, properties and application in the fast removal of heavy-metal ions, Chem. Commun. 47 (2011) 5891–5893, https://doi.org/10.1039/c1cc11640a.
[53] N. Kataria, V.K. Garg, Optimization of Pb (II) and Cd (II) adsorption onto ZnO nanoflowers using central composite design: isotherms and kinetics modelling, J. Mol. Liq. 271 (2018) 228–239, https://doi.org/10.1016/j.molliq.2018.08.135.
[54] P. Wang, T. Shen, X. Li, Y. Tang, Y. Li, Magnetic mesoporous calcium carbonate-based nanocomposites for the removal of toxic Pb(II) and Cd(II) ions from water, ACS Appl. Nano Mater. 3 (2020) 1272–1281, https://doi.org/10.1021/acsanm.9b02036.
[55] Y. Han, T. Nishimura, T. Kato, Morphology tuning in the formation of vaterite crystal thin films with thermoresponsive poly(*N*-isopropylacrylamide) brush matrices, CrystEngComm 16 (2014) 3540–3547, https://doi.org/10.1039/C3CE42646G.
[56] D. Li, L. Ouyang, L. Yao, L. Zhu, X. Jiang, H. Tang, In situ SERS monitoring the visible light photocatalytic degradation of nile blue on Ag@AgCl single hollow cube as a microreactor, ChemistrySelect 3 (2018) 428–435, https://doi.org/10.1002/slct.201702545.
[57] Y. Sano, Y. Hao, F. Kuwahara, Development of an electrolysis based system to continuously recover magnesium from seawater, Heliyon 4 (2018), e00923, https://doi.org/10.1016/j.heliyon.2018.e00923.
[58] M.M.M.G.P. Mantilaka, H.M.T.G.A. Pitawala, D.G.G.P. Karunaratne, R.M. G. Rajapakse, Nanocrystalline magnesium oxide from dolomite via poly(acrylate) stabilized magnesium hydroxide colloids, Colloids Surf. A Physicochem. Eng. Asp. 443 (2014) 201–208, https://doi.org/10.1016/j.colsurfa.2013.11.020.
[59] D.K. Chanda, A. Samanta, A. Dey, P.S. Das, A.K. Mukhopadhyay, Nanoflower, nanoplatelet and nanocapsule $Mg(OH)_2$ powders for adsorption of CO_2 gas, J. Mater. Sci. 52 (2017) 4910–4922, https://doi.org/10.1007/s10853-016-0728-4.
[60] K. Jokai, T. Nakamura, S. Okabe, S. Ishii, Simultaneous removal of nitrate and heavy metals in a continuous flow nitrate-dependent ferrous iron oxidation (NDFO) bioreactor, Chemosphere 262 (2021), 127838, https://doi.org/10.1016/j.chemosphere.2020.127838.
[61] R. Dalvand, E. Kianpour, H. Tahzibi, S. Azizian, MgO nano-sheets for adsorption of anionic dyes from aqueous solution: equilibrium and kinetics studies, , Surf. Interfaces 21 (2020), 100722, https://doi.org/10.1016/j.surfin.2020.100722.
[62] N. Ponomarev, O. Pastushok, E. Repo, B. Doshi, M. Sillanpää, Lignin-based magnesium hydroxide nanocomposite: synthesis and application for the removal of potentially toxic metals from aqueous solution, ACS Appl. Nano Mater. 2 (2019) 5492–5503, https://doi.org/10.1021/acsanm.9b01083.